

# Chiral and deconfinement thermal transitions at finite quark spin polarization in lattice QCD simulations

V. V. Braguta,<sup>1,\*</sup> M. N. Chernodub,<sup>2,3,†</sup> and A. A. Roenko<sup>1,‡</sup>

<sup>1</sup>*Bogoliubov Laboratory of Theoretical Physics, Joint Institute for Nuclear Research, Dubna, 141980 Russia*

<sup>2</sup>*Institut Denis Poisson UMR 7013, Université de Tours, 37200 France*

<sup>3</sup>*Department of Physics, West University of Timișoara,  
Bd. Vasile Pârvan 4, Timișoara 300223, Romania*

(Dated: March 25, 2025)

We study the effect of finite spin quark density on the chiral and deconfinement thermal transitions using numerical simulations of lattice QCD with two dynamical light quarks. The finite spin density is introduced by the quark spin potential in the canonical formulation of the spin operator. We show that both chiral and deconfinement temperatures are decreasing functions of the spin potential. We determine the parabolic curvatures of transition temperatures in a limit of physical quark masses.

## I. INTRODUCTION

Properties of spin degrees of freedom in quark-gluon plasma have attracted significant attention [1]. The interplay of rotation, vorticity, and spins of quarks leads to a series of experimentally observable effects in this strongly interacting medium that emerges in relativistic heavy-ion collisions [2]. On the theoretical side, the investigation of the spin dynamics establishes new links between quantum field theory, thermodynamics, hydrodynamics, and relativistic many-body systems [3–5].

Importantly, the spin effects in quark-gluon plasma can also be accessed experimentally, for example, via measuring the polarization of  $\Lambda$  and  $\bar{\Lambda}$  hyperons that are produced in non-central heavy-ion collisions [6]. The alignment of spins of these particles with the direction of the angular momentum of the quark-gluon plasma provides experimental evidence for the coupling between macroscopic rotation and microscopic spin degrees of freedom of quarks [1]. This high-energy phenomenon has deep roots in the celebrated Barnett effect, which was observed more than a century ago: a rotating ferromagnet gets magnetized by rotation via an alignment of intrinsic spins parallel to the rotation axis [7].

Thermodynamic properties of vortical quark-gluon plasmas have been subjected to intensive theoretical investigation in various effective analytical models [8–27]. The effect of uniform rotation on the thermal phase transition has also been investigated numerically, both in purely gluonic lattice Yang-Mills theory [28–35] and in lattice QCD with dynamical quarks [36, 37]. A comparison between theoretical and numerical approaches revealed a profound disagreement between predictions of the most theoretical models and the numerical results of first-principle simulations: while the effective infrared models with original, rotation-independent parameters indicate that the critical temperatures should drop in the

vortical plasma, the numerical simulations demonstrate that both deconfinement and chiral transition temperatures, on the contrary, rise with increased rotation (see discussions in Refs. [16, 38]). A thorough numerical study of Refs. [35, 36] revealed that this contradiction is a result of the non-perturbative dynamics of gluons, which is difficult to take into account in analytical models.

A window on the properties of the vortical quark-gluon plasma can be opened by investigation of the spin polarization of quarks, which can serve a spin-sensitive probe of the non-perturbative dynamics of the gluonic component. A finite spin polarization corresponds to a presence of a finite density of spins of quarks in quark-gluon plasma. In a statistical ensemble, a quark spin density can be introduced via a spin potential in exactly the same spirit as a finite baryon density is described via a finite baryon chemical potential. The spin potential shares a distant similarity with the axial and helical chemical potentials [39, 40]. In our article, we study the effect of the finite quark spin density on the phase diagram of QCD using first-principle Monte Carlo simulations. We concentrate our attention on the chiral and deconfinement thermal transitions.

It is important to stress the existence of an ambiguity in the very definition of a spin tensor that determines the local spin degrees of freedom. This ambiguity appears as a result of the pseudogauge symmetry [41–43], which could potentially be fixed by observing that a concrete expression for the spin tensor can be linked to the particularities of the spin interactions in the system [44]. Following the latter article, we will use, in the field-theoretical language, the canonical definition of the spin tensor, which can directly be derived via Noether's theorem applied to Dirac fermions.

The structure of the paper is as follows. In Section II, we introduce the spin potential in the Dirac Lagrangian and define the notion of the curvature of the phase transition with respect to the spin potential. Section III is devoted to the description of our numerical setup and the presentation of the results of our Monte Carlo simulations. The last section includes a brief discussion and conclusions.

\* [vvbraguta@theor.jinr.ru](mailto:vvbraguta@theor.jinr.ru)

† [maxim.chernodub@univ-tours.fr](mailto:maxim.chernodub@univ-tours.fr)

‡ [roenko@theor.jinr.ru](mailto:roenko@theor.jinr.ru)

## II. FINITE QUARK SPIN DENSITY

### A. Introducing quark spin potential

Using numerical Monte Carlo simulations, we study the phase diagram of QCD at finite spin density of quarks. The concept of the quark spin density is somewhat similar to a finite baryonic density associated with the quark degrees of freedom. The latter can be achieved by introducing the quark chemical potential  $\mu_q$ , which is conjugated to the quark number density. Analogously, the finite spin density of quarks can effectively be described by the spin potential  $\mu_\Sigma$  which is thermodynamically conjugated with the density of quark spins. A thermodynamic ensemble of quarks characterized by a finite spin potential  $\mu_\Sigma \neq 0$  possesses nonzero densities of spin-polarized quarks and anti-quarks such that the total baryonic charge vanishes while the spin polarization is nonzero. In other words, in such a configuration, the total numbers of quarks and anti-quarks are equal to each other, implying that the positive baryonic charge of quarks cancels by the negative baryonic charge of anti-quarks. However, the spins of quarks and anti-quarks add up, so that the total spin in this baryon-neutral configuration is nonzero.

The quark spin density can be described by the following term in the Dirac Lagrangian:

$$\delta_\Sigma \mathcal{L}_q = \mu_{\alpha,\mu\nu} \bar{\psi} \mathcal{S}^{\alpha,\mu\nu} \psi, \quad (1)$$

where we introduced the relativistic spin density matrix,

$$\mathcal{S}^{\alpha,\mu\nu} = \frac{1}{2} \{ \gamma^\alpha, \Sigma^{\mu\nu} \}, \quad \Sigma^{\mu\nu} = \frac{i}{4} [\gamma^\mu, \gamma^\nu], \quad (2)$$

which plays the role of the canonical relativistic spin current operator for spin-1/2 Dirac fermions. The associated background relativistic spin field  $\mu_{\alpha,\mu\nu}$  introduces a finite spin density and a finite spin current in the system.

Without losing generality, we consider the spins of quarks polarized along the  $z$  axis in a certain inertial reference frame. We choose the background relativistic spin field as follows:

$$\mu_{\alpha,\mu\nu} = \frac{\mu_\Sigma}{2} \delta_{\alpha 0} (\delta_{\mu 1} \delta_{\nu 2} - \delta_{\nu 1} \delta_{\mu 2}), \quad (3)$$

with all other components vanishing. We use the Minkowski metric  $g = \text{diag}(1, -1, -1, -1)$ .

The Lagrangian (1) introduces a finite quark-anti-quark density with their spins polarized along the  $z$  direction, with the global spin polarization, controlled by the spin potential  $\mu_\Sigma$ . With Eqs. (2) and (3) in place, the simplified Lagrangian (1) gets the following form:

$$\delta_\Sigma \mathcal{L}_q = \mu_\Sigma \bar{\psi} \gamma^0 \Sigma^{12} \psi. \quad (4)$$

In the Dirac representation, the matrix in the above equation has a diagonal form:

$$\gamma^0 \Sigma^{12} \equiv \mathcal{S}^{0,12} \equiv -\mathcal{S}^{0,21} = \frac{1}{2} \gamma^3 \gamma^5$$

$$= \text{diag}\left(+\frac{1}{2}, -\frac{1}{2}, -\frac{1}{2}, +\frac{1}{2}\right). \quad (5)$$

The quantity  $\mu_\Sigma$  is called ‘‘spin potential’’ as it serves as a potential energy for spin coordinate as and also has a certain similarity with a chemical potential<sup>1</sup>: one needs to use the  $\delta E_\uparrow = +\mu_\Sigma/2$  amount of energy to add a spin-1/2 state that points up along the  $z$  axis and one requires to invest  $\delta E_\downarrow = -\mu_\Sigma/2$  energy to add a spin-1/2 state that points down.

Thus, the spin potential  $\mu_\Sigma$  of relativistic fermions is a thermodynamic quantity that describes the energy difference between adding a spin-1/2 particle with one orientation of a spin versus the other to a system of relativistic fermions,  $\mu_\Sigma = \delta E_\uparrow - \delta E_\downarrow$ . In other words, it expresses a tendency to favor one spin state over the other, and it is a way to account for the spin degree of freedom in the system.

By construction, the notion of the spin potential  $\mu_\Sigma$  is somewhat similar to the notion of the angular velocity  $\Omega$  that characterizes a uniformly rotating system. Indeed, in a reference frame that co-rotates together with the system with angular velocity  $\mathbf{\Omega} = \Omega \mathbf{e}_z$  about the  $z$  axis, the rotation affects the quark Lagrangian by shifting it with the following term (see, for example, a derivation in Ref. [8] or Ref. [10]):

$$\delta_\Omega \mathcal{L}_q = \Omega \bar{\psi} [i(-x\partial_y + y\partial_x) + \gamma^0 \Sigma^{12}] \psi, \quad (6)$$

where the first term represents an orbital momentum of the quarks while the second term corresponds to an effect of global uniform rotation on the quark spin. Identifying for a brief moment  $\Omega = \mu_\Sigma$ , we find that the spin-polarization term for the orbital motion in Eq. (6) coincides precisely with the Lagrangian term that describes the spin polarization in the non-rotating medium (4).

The orbital motion of the quarks is, evidently, absent in our case because we aim to study a spin-polarized but non-rotating medium (4). Our approach has, thus, an advantage that it can be studied in the thermodynamic limit since the spin polarization itself does not cause the causality problem that requires restricting the rotating system to be located entirely within a light cylinder [45].

Before continuing further, it is important to stress that we consider the spin polarization imposed only on quark fields. Spins of gluons are not directly effected by our background. However, it is not excluded (and, moreover, it is quite plausible) that the polarized quark medium does affect the gluon spin polarization indirectly, via quark loops, as the spins of quarks transfer to the spins of gluons and vice versa.

### B. Curvature of the phase transition

In the imaginary time formalism, the quark spin potential becomes an imaginary quantity after the Wick ro-

<sup>1</sup> Following Ref. [1], we call  $\mu_\Sigma$  a spin potential and not a spin chemical potential because the spin is not a conserved quantity.

tation, similarly to the baryon chemical potential. Due to the notorious sign problem, Monte Carlo simulations with a real spin potential in the Wick-rotated Euclidean field theory are impossible. Therefore, following our experience with the quark chemical potential, we proceed by introducing the imaginary spin potential,

$$\mu_\Sigma = i\mu_\Sigma^{\text{I}}, \quad (7)$$

and then use an analytical continuation from imaginary to real values of the spin potential for our results obtained in Monte Carlo simulations.

The procedure of the analytical continuation is justified at small values of the spin potential  $\mu_\Sigma^{\text{I}}$ . In our paper, we aim to find the curvature  $\kappa_\Sigma$  of the deconfinement ( $\ell = L$ ) and chiral ( $\ell = \psi$ ) phase transitions that determine the behavior of the corresponding transition temperatures:

$$\frac{T_c^\ell(\mu_\Sigma^{\text{I}})}{T_c^\ell(0)} = 1 + \kappa_\Sigma^\ell \left( \frac{\mu_\Sigma^{\text{I}}}{T_c(0)} \right)^2 + \dots, \quad [\ell = L, \psi], \quad (8)$$

where higher-order terms are shown by the ellipsis.

Analytically continuing the parabolic function (8) back to the real-valued quark spin potential,  $\mu_\Sigma^{\text{I}} \rightarrow i\mu_\Sigma$ , we get the behavior of the transition temperatures as a function of  $\mu_\Sigma$ :

$$\frac{T_c^\ell(\mu_\Sigma)}{T_c(0)} = 1 - \kappa_\Sigma^\ell \left( \frac{\mu_\Sigma}{T_c(0)} \right)^2 + \dots, \quad [\ell = L, \psi]. \quad (9)$$

The spin curvature  $\kappa_\Sigma$  describes how the presence of small quark density affects the deconfining transition: a positive (negative)  $\kappa_\Sigma$  would imply that the transition temperature diminishes (grows) as the spin density increases. In this article, we compute numerically the thermal ‘‘spin’’ curvature  $\kappa_\Sigma$  of the deconfining phase transition (9). Surprisingly, our simulations demonstrate that the parabolic regime of Eqs. (8) and (9) extends well beyond the region of small spin potentials.

At the end of this section, we notice a curious analogy that emerges, at zero temperature, between the systems described, on one side, by the imaginary quark spin potential  $\mu_\Sigma^{\text{I}}$  in the Euclidean spacetime and, on the other side, the axial (chiral) chemical potential,  $\mu_A$  both in Euclidean and Minkowski spacetimes (we remind the reader that a finite axial density does not lead to the sign problem). According to Eq. (5), a finite spin polarization along a spatial direction is proportional to the axial current density along the same direction,  $j_A^3 = \bar{\psi}\gamma^3\gamma^5\psi \equiv 2\bar{\psi}\gamma^0\Sigma^{12}\psi$ , where we took the spatial direction  $\mu = 3$  for definiteness. Therefore, a spin potential generates an axial current along the corresponding spatial direction. At zero temperature Euclidean field theory, the spatial directions and the imaginary time direction are equivalent. Therefore, the spin polarization generated by the spin potential  $\mu_\Sigma^{\text{I}}$  is equivalent to the axial density produced by the axial chemical potential  $\mu_A = \mu_\Sigma^{\text{I}}/2$ .

QCD at finite axial chemical potential  $\mu_A$  was studied intensively both theoretically (see, for instance, papers [46–51]) and within lattice simulations [52–54]. Among the results related to this paper, one could mention the chiral catalysis phenomenon [47], which enhances the chiral condensate in the presence of a non-zero axial (chiral) density generated by a finite axial chemical potential  $\mu_A$ . In addition, the QCD string tension is enhanced as the chiral density gets larger [54]. As a result, the critical temperatures of chiral and deconfinement transitions are increased as the chiral chemical potential gets larger [52, 53]. Because of the mentioned isotropy of the Euclidean spacetime at zero temperature, the same effect also holds a finite spin potential  $\mu_\Sigma^{\text{I}}$ . Since the increasing spin potential enhances the chiral condensate and the confinement property, it works oppositely to the effect of thermal fluctuations that tend to diminish both the chiral condensate and decrease the tension of the confining string. This observation suggests that the transition temperature rises with the increase of  $\mu_\Sigma^{\text{I}}$ , thus implying  $\kappa_\Sigma > 0$  in Eq. (8). Below, we calculate  $\kappa_\Sigma$  numerically using first-principle lattice simulations.

### III. SIMULATIONS AT FINITE SPIN DENSITY

#### A. Lattice setup

The incorporation of a quark spin potential into the lattice QCD action shares some similarity with imposing a uniform rotational background, albeit with two significant simplifications.

First of all, we stress that the quark spin potential, as it follows from the name of this quantity, is applied explicitly only to the quark degrees of freedom. Therefore, the gluons are not subjected *directly* to rotation. In notations of Ref. [36], the angular velocity of gluon fields is zero,  $\Omega_G = 0$ .

Moreover, in order to impose the quark spin potential, we should not rotate quarks in the orbital sense. In continuum notations, the Euclidean fermionic action under the rigid rotation with the angular velocity  $\Omega$  has the following form:

$$S_F = \int d^4x \bar{\psi} \left[ \gamma^x D_x + \gamma^y D_y + \gamma^z D_z \right. \quad (10)$$

$$\left. + \gamma^\tau (D_\tau + i\mu_\Sigma \Sigma^{12}) + m \right] \psi, \quad (11)$$

where  $D_\mu$  is the covariant derivative and  $\Sigma^{\mu\nu}$  is the spin matrix defined in Eq. (2).

In action (11), the spin polarization is taken into account by the  $\Sigma^{12}$  term, while the orbital rotation may be encoded in the change in the Dirac gamma matrices [55]. Since the orbital term is not needed for our aims, the gamma matrices remain unmodified:  $\gamma^x = \gamma^1$ ,  $\gamma^y = \gamma^2$ ,  $\gamma^z = \gamma^3$ , and  $\gamma^\tau = \gamma^4$ , so that the quarks do not perform the orbital motion. Thus, in order to incorporate

the spin polarization, we need only the spin-rotation coupling term  $i\gamma^\tau \Omega \Sigma^{12}/2$ , where we take  $\Omega \rightarrow \mu_\Sigma$ . Notice that we omitted above an index of the chemical potential,  $\mu_s \equiv \mu_{s;z}$  since the spin is assumed to be induced in the  $z$  direction.

Technically, the numerical simulations of lattice QCD at finite quark spin density have noticeable simplifications compared to the simulations of quark-gluon matter in the rotating frame: the system is homogeneous, and there is no need to impose non-trivial boundary conditions in  $x, y$ -direction in order to enforce the causality property. Thus, the simulations at finite quark spin density are rather similar to QCD at finite baryon density or chiral chemical potential, and, at the same time, they are similar to the simulations of the rotating QCD in which the rotating gluonic and rotating orbital quark contributions are omitted. In order to simplify the technical implementation of the spin potential and make it possible to compare the results of vortical and quark-spin-polarized plasmas, we used a modification of the same lattice action, as in our ongoing study of rotating QCD [36], with vortical gluon and orbital quark parts excluded.

We discretize the gluon part of the action using the renormalization-group improved (Iwasaki) lattice action [56], which is unaffected by spin density:

$$S_G = \beta \sum_x \left( c_0 \sum_{\mu < \nu} W_{\mu\nu}^{1 \times 1} + c_1 \sum_{\mu \neq \nu} W_{\mu\nu}^{1 \times 2} \right), \quad (12)$$

with the lattice couplings  $\beta = 6/g^2$ ,  $c_0 = 1 - 8c_1$ , and  $c_1 = -0.331$ . The gauge field enters via

$$W_{\mu\nu}^{1 \times 1}(x) = 1 - \frac{1}{3} \text{Re Tr } \bar{U}_{\mu\nu}(x), \quad (13)$$

$$W_{\mu\nu}^{1 \times 2}(x) = 1 - \frac{1}{3} \text{Re Tr } R_{\mu\nu}(x), \quad (14)$$

where  $\bar{U}_{\mu\nu}(x)$  denotes the clover-type average of four plaquettes and  $R_{\mu\nu}(x)$  represents a rectangular loop [29].

The gauge action is supplemented by the  $N_f = 2$  clover-improved action for Wilson fermions [57], which now incorporates the imaginary spin potential  $\mu_\Sigma^1$ :

$$S_F = \sum_{f=u,d} \sum_{x_1, x_2} \bar{\psi}^f(x_1) M_{x_1, x_2} \psi^f(x_2), \quad (15)$$

with the matrix

$$\begin{aligned} M_{x_1, x_2} &= \delta_{x_1, x_2} - \\ &- \kappa \left[ \sum_{\mu=x,y,z} \left( (1 - \gamma^\mu) T_{\mu+} + (1 + \gamma^\mu) T_{\mu-} \right) + \right. \\ &+ (1 - \gamma^\tau) \exp \left( ia\mu_\Sigma^1 \Sigma^{12} \right) T_{\tau+} + \\ &+ \left. (1 + \gamma^\tau) \exp \left( -ia\mu_\Sigma^1 \Sigma^{12} \right) T_{\tau-} \right] - \\ &- \delta_{x_1, x_2} c_{SW} \kappa \sum_{\mu < \nu} \sigma_{\mu\nu} F_{\mu\nu}, \end{aligned} \quad (16)$$

where  $\kappa = 1/(8 + 2am)$ ,  $T_{\mu+} = U_\mu(x_1) \delta_{x_1+\mu, x_2}$ ,  $T_{\mu-} = U_\mu^\dagger(x_1) \delta_{x_1-\mu, x_2}$  and  $F_{\mu\nu} = (\bar{U}_{\mu\nu} - \bar{U}_{\mu\nu}^\dagger)/8i$ . For the clover coefficient, we adopt the mean-field value  $c_{SW} = (1 - W^{1 \times 1})^{-3/4} = (1 - 0.8412/\beta)^{-3/4}$  following Refs. [58, 59] and then substitute a one-loop result for the plaquette [56].

For this lattice action, the masses of light mesons were calculated for a wide range of simulation parameters in Refs. [60–63]. We reanalyze that data to restore the lines of constant physics, and our interpolation results are consistent with previous studies [58, 62] within systematic uncertainties. Simulations are performed on lattices of the size  $4 \times 16^3$ ,  $5 \times 20^3$ ,  $6 \times 24^3$  for meson mass ratios  $m_{PS}/m_V = 0.60, \dots, 0.85$ . Note that in rotating QCD, we found that the fermionic and gluonic degrees of freedom have opposite effects on the transition temperature [36]. Therefore, the dependence of the results on the pion mass – which controls the dynamical properties of fermions – is of a particular interest.

## B. Observables

At zero baryon density, quark-gluon matter can exist in two distinct phases. The low-temperature phase possesses the color confinement property and exhibits the chiral symmetry breaking, implying that the physical degrees of freedom are massive, colorless hadronic states. The high-temperature phase is the quark-gluon plasma, in which the quarks and gluons are deconfined and the chiral symmetry is restored. At real physical quark masses, the transition between these phases is a smooth crossover [64], which possesses no thermodynamic singularity. In our paper, we are interested both in confining and chiral properties of quark-spin-polarized QCD.

In the absence of dynamical quarks, QCD is reduced to Yang-Mills theory, where the transition between the confining and deconfining phases is a true thermodynamic phase transition of the first order. The phases are distinguished by the expectation value of the Polyakov loop, which is an order parameter of the deconfinement phase:

$$L = \langle |L_{\text{bulk}}| \rangle, \quad L_{\text{bulk}} = \frac{1}{V} \int d^3r L(\mathbf{r}), \quad (17)$$

$$L(\mathbf{r}) = \text{Tr } \mathcal{P} \exp \left( \oint_0^{1/T} d\tau A_4(\tau, \mathbf{r}) \right), \quad (18)$$

where  $\mathcal{P}$  is a path ordering operator. Notice that both confining and deconfining regimes represent homogeneous phases so that the expectation value of the local Polyakov loop  $\langle L(\mathbf{r}) \rangle$  does not depend on the spatial point  $\mathbf{r}$ . The system is expected to maintain the spatial homogeneity also at small values of the spin potential.

In the low-temperature confinement phase, the expectation value of the Polyakov loop (18) vanishes,  $L = 0$ , indicating that the free energy of a single heavy quark,  $F_Q = -T \ln |L|$  diverges ( $F_Q \rightarrow \infty$ ). Therefore, free isolated quarks do not exist in the low-temperature phase.

The vanishing expectation value of the Polyakov loop implies that the center  $\mathbb{Z}_3$  global symmetry is respected by the ground state  $L = 0$ , which is invariant under the global transformations  $L \rightarrow e^{i2\pi n/3} L$ , with  $n = 0, 1, 2$ .

In the high-temperature phase, the Polyakov loop does not vanish,  $L \neq 0$ , and the center  $\mathbb{Z}_3$  symmetry is broken by a nonzero value of the Polyakov loop. Thus, the free energy of a single quark is a finite quantity,  $F_Q < \infty$ , and quarks can propagate without being confined to colorless bound states.

In the presence of dynamical matter fields, the center  $\mathbb{Z}_3$  symmetry is no more respected. Therefore, the Polyakov loop becomes only an approximate order parameter of the deconfining phase transition of QCD. Despite this apparent inconsistency, we can still use the inflection point of the Polyakov loop expectation value as a function of temperature to determine the crossover position. Alternatively, we can associate this transition temperature with the position of the peak of the susceptibility of the bulk Polyakov loop (17),

$$\chi_L = N_s^3 (\langle |L_{\text{bulk}}|^2 \rangle - \langle |L_{\text{bulk}}| \rangle^2), \quad (19)$$

where  $N_s$  is a lattice size in spatial directions. While both these formal definitions give comparable values, given a substantial width of the transition in the thermodynamic limit, we will use the maximum of the susceptibility (19) in our determination of the pseudocritical temperature of the deconfining transition.

On the lattice, the local Polyakov loop (18) has the following definition:

$$L(\mathbf{r}) = \left\langle \frac{1}{3} \text{Tr} \left[ \prod_{\tau=0}^{N_t-1} U_4(\tau, \mathbf{r}) \right] \right\rangle, \quad (20)$$

where  $U_4(\tau, \mathbf{r})$  is the link variable in the temporal direction. The bulk expectation value is given by Eq. (17), where the integral is replaced by a sum over the lattice sites.

In QCD with dynamical quarks, the deconfinement crossover is accompanied by the restoration of chiral symmetry. For the chiral crossover, we determine the pseudocritical temperature using the (disconnected) chiral susceptibility:

$$\chi_{\psi\psi}^{\text{disc}} = \frac{N_f T}{V} \left[ \langle \text{Tr}(M^{-1})^2 \rangle - \langle \text{Tr}(M^{-1}) \rangle^2 \right], \quad (21)$$

which has a peak at the transition point.

### C. Results

We show the expectation value of the bulk Polyakov loop  $L$  as a function of temperature in Fig. 1. The data are presented for a single value of the pseudoscalar meson mass, encoded in the ratio  $m_{\text{PS}}/m_V = 0.65$ , and for various values of the imaginary spin potential  $\mu_\Sigma^I$  at the temporal extension of the lattice  $N_t = 5$ .

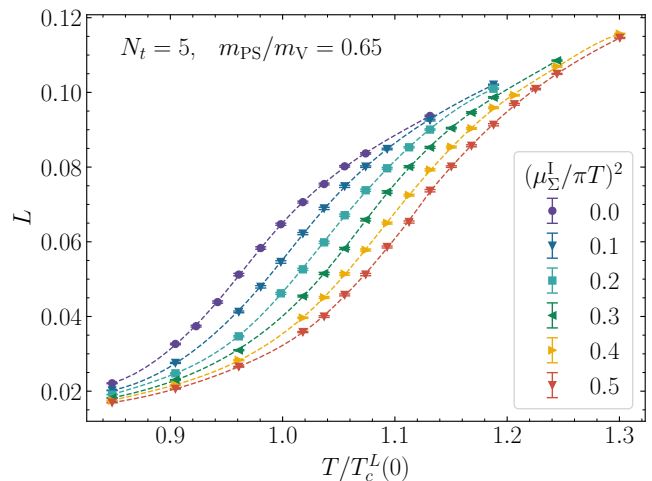


Figure 1. Expectation value of the Polyakov loop as a function of temperature  $T$  for various values of the spin potential  $\mu_\Sigma$ . The calculations were performed at the temporal extension of the lattice  $N_t = 5$  at the meson ratio  $m_{\text{PS}}/m_V = 0.65$ . Temperature and spin chemical potential  $\mu_\Sigma$  are given in units of the deconfinement crossover temperature at vanishing spin density,  $T_c^L(0)$ . The dotted lines are drawn to guide the eye.

An increasing imaginary spin potential leads to a decrease of the Polyakov loop at fixed temperature while keeping the low-temperature and high-temperature asymptotics largely intact. This behavior implies that at a finite spin density, the transition shifts to the higher temperatures as compared to the case with vanishing spin density.

The transition temperature for the deconfinement transition can be associated with the maximum of the Polyakov loop susceptibility (19) as shown in Fig. 2(top). Similarly, the chiral transition point can be obtained from the maximum of the (disconnected) susceptibility of the chiral condensate, Fig. 2(bottom).

Both transition temperatures are shown in Fig. 3 as functions of the imaginary chemical potential  $\mu_\Sigma^I$ , for two meson mass ratios  $m_{\text{PS}}/m_V$  and various temporal extensions of the lattice  $N_t = 4, 5, 6$ . At fixed temperature  $T = 1/(N_t a)$ , as the number of sites  $N_t$  in the imaginary temporal direction increases, the lattice spacing decreases, thus allowing us to test the scaling of the data in the ultraviolet limit. The data in Fig. 3 indicate weak dependence of the transition temperature on the ultraviolet lattice cutoff played by the lattice spacing  $a$ . Moreover, it shows a quadratic behavior of the transition temperature on the imaginary spin potential in consistency with the expected behavior (8).

In order to find the curvatures of the deconfinement and chiral transitions, we fit the data for the pseudocritical temperatures by the following function of the imaginary spin potential  $\mu_\Sigma^I$ :

$$T_c^\ell(\mu_\Sigma^I) = T_c^\ell(0) \left[ 1 + \kappa_\Sigma^\ell \left( \frac{\mu_\Sigma^I}{T} \right)^2 \right], \quad (22)$$

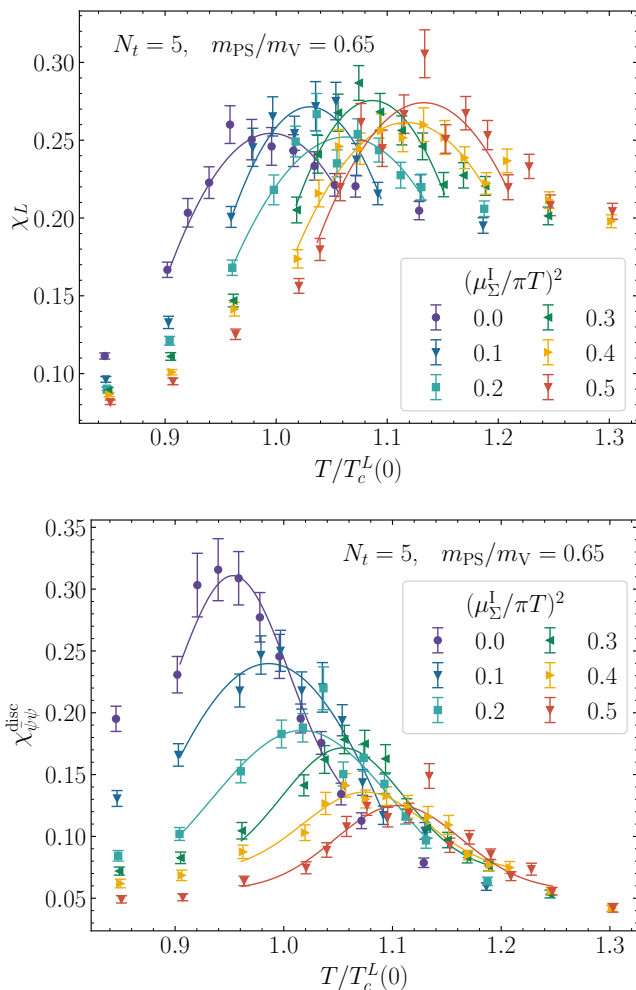


Figure 2. The same as in Fig. 1 but for the susceptibilities of (top) the Polyakov loop and (bottom) the chiral condensate. The solid lines correspond to the best fits of the numerical data by a Gaussian function.

where the index  $\ell$  labels the deconfinement ( $\ell = L$ ) and chiral ( $\ell = \psi$ ) pseudocritical temperatures. For each transition  $\ell = L, \psi$ , the fitting function (22) has two fitting parameters that fix the critical temperature  $T_c^\ell(0)$  at a vanishing imaginary spin chemical potential  $\mu_\Sigma^I$ , and the curvature  $\kappa_\Sigma^\ell$  of the transition at small values of  $\mu_\Sigma^I$ . For convenience, the data for all pseudocritical temperatures in Fig. 3 are normalized by the temperature  $T_c^L(0)$  of the deconfinement crossover at vanishing spin density. Notice that up to inessential quartic terms, Eq. (22) can also be rewritten in the more familiar form (8).

The dependence of the transition temperature on the imaginary spin potential for all available ratios of the meson masses  $m_{PS}/m_V$  is summarized in Fig. 4. The data point out that at each fixed value of the ratio, the transition temperature is a parabolic function of the imaginary spin potential.

The best fits of the data for the transition temperature by the quadratic polynomial (8) of the imaginary spin po-

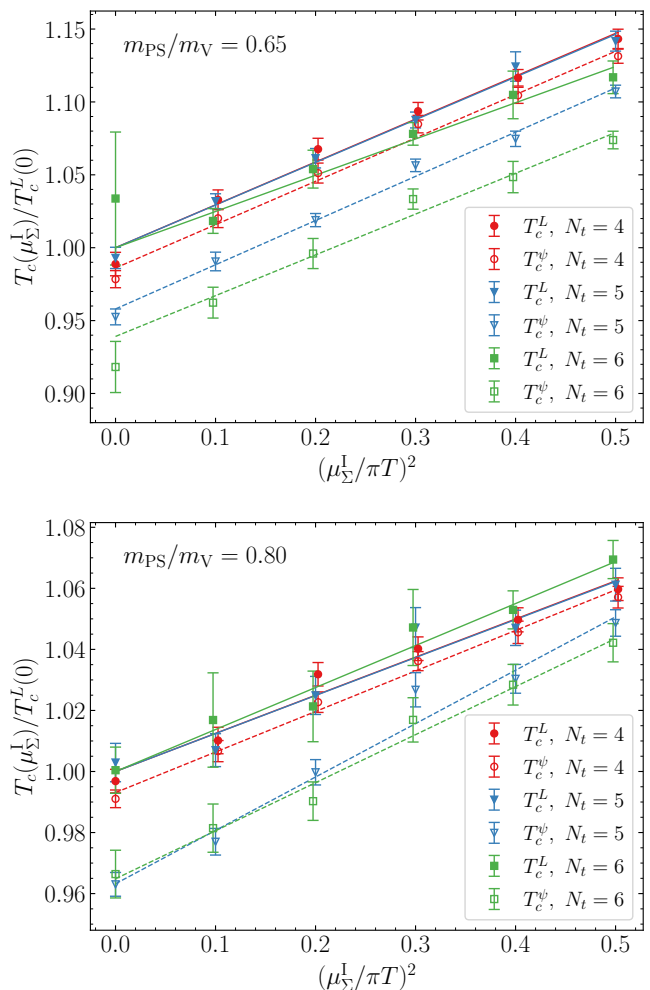


Figure 3. Transition temperature  $T_c$  of the deconfinement (filled markers) and chiral (empty markers) crossovers at the meson ratios (top)  $m_{PS}/m_V = 0.65$  and (bottom)  $m_{PS}/m_V = 0.8$  as a function of the squared imaginary spin potential  $\mu_\Sigma^I$  (normalized by  $\pi T$ ) for the temporal extensions  $N_t = 4, 5, 6$ . The solid lines represent the linear fits given by Eq. (22). For convenience, the data are normalized by the fit coefficient  $T_c^L(0)$  (i.e., by the critical temperature of the deconfinement transition in the absence of the spin polarization).

tential are shown in Fig. 4 by solid lines. These fits allow us to obtain the dependence of the parabolic slope  $\kappa_\Sigma$  as a function of the (squared) ratio of the meson masses, shown in Fig. 5.

We immediately notice from Fig. 5 that the curvature  $\kappa_\Sigma$  of the spin-related shift in the transition temperature is a positive quantity. It implies, according to the analytical continuation (8), that the transition temperature decreases as the spin density becomes higher.

Furthermore, we observe that as the pion mass increases (i.e., as the ratio  $m_{PS}/m_V$  grows), the curvature  $\kappa_\Sigma$  decreases. This behavior is anticipated, as the contributions of quark loop effects diminish with increasing quark mass. At sufficiently high masses, the impact of quarks on gluon dynamics, including the transfer of spin

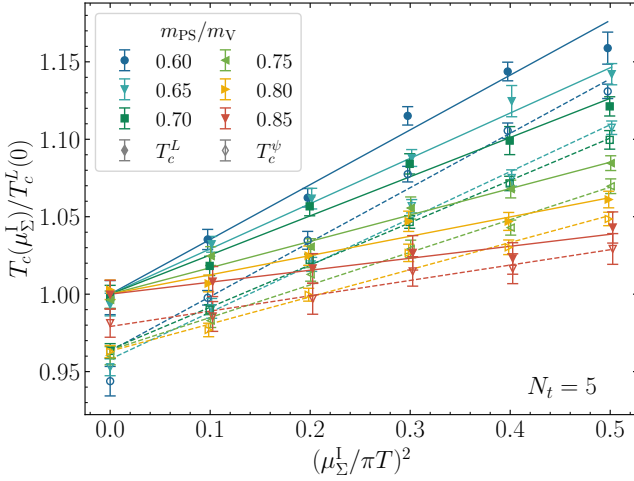


Figure 4. Transition temperatures  $T_c^L$  and  $T_c^\psi$  as a function of the (normalized) squared spin potential  $\mu_\Sigma^I$  for various ratios of the meson masses  $m_{\text{PS}}/m_V$  at  $N_t = 5$  lattice. The solid (dotted) lines represent the linear fits for deconfinement (chiral) pseudocritical temperatures given by Eq. (22). The data are normalized by the critical temperature of deconfinement transition,  $T_c^L(0)$ .

polarization from quarks to gluons, becomes negligible. This expectation is well corroborated by our data presented in Fig. 4.

The dependence of the curvatures  $\kappa_\Sigma^\ell$  ( $\ell = L, \psi$ ) on the pion mass ratio can be well described by a simple parabolic dependence on the ratio of the meson masses:

$$\kappa_\Sigma^\ell(\xi) = \varkappa_\Sigma^\ell + \gamma_\Sigma^\ell \xi^2, \quad \xi = \frac{m_{\text{PS}}}{m_V}. \quad (23)$$

The best fits of the curvatures  $\kappa_\Sigma^\ell$  with  $\ell = L, \psi$  by the function (23) are shown in Fig. 5. The best-fit parameters are:

$$\varkappa_\Sigma^L = 0.0635(37), \quad \gamma_\Sigma^L = -0.0795(67), \quad (24)$$

$$\varkappa_\Sigma^\psi = 0.0616(29), \quad \gamma_\Sigma^\psi = -0.0686(53), \quad (25)$$

implying that at the physical ratio of the masses, the curvature of the spin-induced inhibition of the deconfinement temperature is:

$$\kappa_\Sigma^L(\text{phys}) = 0.0610(35), \quad (26a)$$

$$\kappa_\Sigma^\psi(\text{phys}) = 0.0595(27), \quad (26b)$$

$$\left[ \text{at} \left( \frac{m_{\text{PS}}}{m_V} \right)_{\text{phys}} = 0.175 \right].$$

The influence of the finite spin density on the deconfining transition is qualitatively similar to the effect produced by a non-vanishing baryonic density, since a non-vanishing baryon chemical potential lowers the temperature of the deconfinement transition as well.

It is interesting to compare the curvatures in the phase transition generated by finite spin and finite baryon densities. We can take, as a reasonable reference point, the

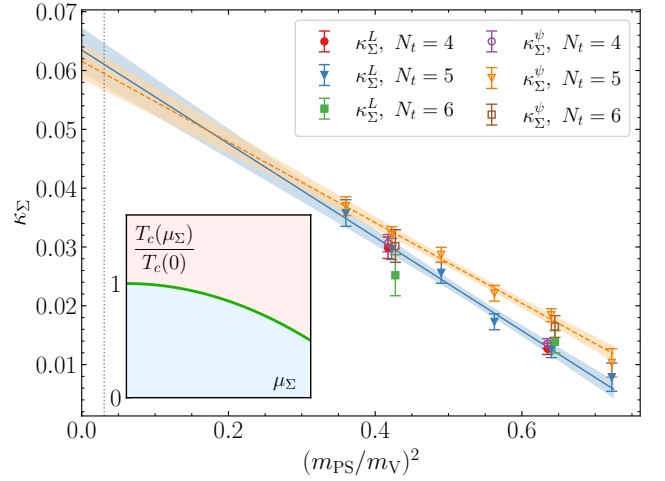


Figure 5. Curvatures of the deconfinement and chiral transitions,  $\kappa_\Sigma^L$  and  $\kappa_\Sigma^\psi$ , respectively, which determine the parabolic dependence (9) of the corresponding transition temperatures  $T_c$  on the spin potential  $\mu_\Sigma^I$ . The transition temperature can be well described by a quadratic function of function (23) of the mesonic mass ratio  $m_{\text{PS}}/m_V$ . The solid line represents the best fit by the parabolic function (23) with the shadowed region denoting the error range of the fit. The vertical dashed line represents the physical value of the meson ratio,  $m_{\text{PS}}/m_V \simeq 0.175$ . The inset shows the qualitative behaviour (9) of the transition temperature  $T_c$  on the spin potential  $\mu_\Sigma$ .

curvature  $\kappa_B$  of the pseudo-critical transition as a function  $T_c(\mu_B)/T_c(0) = 1 - \kappa_B(\mu_B/T_c)^2$  of the baryon chemical potential  $\mu_B$ . Taking as an estimate the continuum-extrapolated result  $\kappa_B = 0.0135(20)$  of Ref. [65] for QCD with  $N_f = 2 + 1$  dynamical quarks and setting, for strange-neutral matter, the relation  $\mu_B = 3\mu_q$  between the baryonic,  $\mu_B$ , and flavor-averaged quark chemical potential  $\mu_q$ , we get  $T_c(\mu_B)/T_c(0) = 1 - \kappa_q(\mu_q/T_c)^2$  with  $\kappa_q = 9\kappa_B$ . Thus, the curvature of the transition temperature associated with the presence of a nonzero quark chemical potential  $\mu_q$  is  $\kappa_q = 0.12(2)$  which is approximately two times larger than the curvatures of the chiral and deconfinement transitions (26). Thus, the effect of a finite spin density on the phase transition is quantitatively similar to the effect of the finite baryonic density.

The effect of a finite isospin quark density on the transition temperature is also similar to the one of the finite quark density: the pseudo-critical temperature diminishes with the increase of the isospin chemical potential [66]. The curvatures of both these transitions are close to each other as well [67]. Thus, we conclude that a finite spin polarization affects both thermal transitions a very similar way as the finite quark density and finite isospin density of quarks.

Despite the similarity mentioned above there is an important difference between chiral and deconfinement thermal transitions at finite baryon and spin densities. This difference can be seen from Fig. 2: imaginary spin

chemical potential noticeably increases the width of the chiral susceptibility thus softening the chiral phase transition, while there is no sign of similar softening for the deconfinement transition. Notice that this property is not observed at finite imaginary baryon chemical potential (see, for instance, the recent paper [68]). Analytically continuing the width of the chiral transition, one can draw a conclusion that the transition becomes more abrupt for real values of spin chemical potential. It might be that at sufficiently large spin density the width of the chiral transition is zero and it might turn to the first order phase transition. Notice, however, that a careful study of this point is beyond the scope of the present paper.

#### IV. CONCLUSIONS

We performed first-principle numerical simulations in the lattice QCD with  $N_f = 2$  dynamical quarks to determine the effect of a finite spin density of quarks on the deconfinement and chiral transitions. The spin density has been introduced by employing a finite spin potential within the canonical definition of the Dirac fermion spin.

Our simulations reveal that a finite spin density of quarks affects the dynamics of gluons and has a measurable impact on the confining and chiral properties of QCD. Thermodynamically, the quark spin density leads to a decrease of the temperatures of the chiral and deconfinement crossover (9), making the spin potential somewhat alike the baryon chemical potential that has a qualitatively similar effect. This similarity can have a physical explanation since an increasing baryonic chemical potential introduces quarks or anti-quarks into the system, favoring the deconfined phase by enhancing the screening of the long-range color potential, confining string breaking, and hadron percolation effects. Likewise, the spin potential introduces quarks and anti-quarks to produce a spin-polarized but globally baryon-neutral medium. The presence of the dynamical quark degrees of freedom in the latter case also leads to color screening and hadronic percolation, which inhibits the confining properties of gluons.

Quantitatively, the inhibition of the confining and chiral-symmetry-breaking properties of quark-gluon matter in the presence of a finite spin polarization of quarks can be described by the dimensionless curvatures,  $\kappa_\Sigma^L$  and  $\kappa_\Sigma^\psi$  associated with the deconfinement and chiral transi-

tions, respectively. We established the effects of the pion mass on the transition temperature and found that at the physical point, the transition curvatures are approximately the same within a small statistical error (26),  $\kappa_\Sigma^L \simeq \kappa_\Sigma^\psi \simeq 0.06$ . The equivalence of the curvatures implies that the presence of the background spin potential does not lead to a splitting of the deconfinement and chiral transitions.

The small magnitude of the curvatures implies that for the phenomenologically relevant values of the spin potential  $\mu_\Sigma = 10$  MeV, the deconfinement and chiral transition temperatures drop only by about 0.03%. To make this estimation, we took into account that in rotating quark-gluon plasma, the magnitude of the spin polarization is expected to be of the order of vorticity which reaches about  $\Omega \simeq 10$  MeV in experiments on heavy-ion collisions [6]. Our results imply that the spin polarization in the quark sector has a significantly smaller influence on the system properties than the rotation effects in gluon sector [31–36]. Despite the tiny effect of a realistic spin density on the bulk thermodynamic transition, our result shows that the spin of quarks affects the deconfining properties of gluons, acting, presumably, via their spins. The existence of the transfer of spin polarization from quark to gluon degrees of freedom may be interesting on its own as it may shed a light to a well-known problem of the proton spin crisis [69].

#### ACKNOWLEDGMENTS

The authors are grateful to Andrey Kotov for useful discussions. The work has been carried out using computing resources of the Federal collective usage center Complex for Simulation and Data Processing for Mega-science Facilities at NRC “Kurchatov Institute”, <http://ckp.nrcki.ru/> and the Supercomputer “Govorun” of Joint Institute for Nuclear Research. The work of VVB and AAR, which consisted of the lattice calculation of the observables used in the paper and interpretation of the data, was supported by the Russian Science Foundation (project no. 23-12-00072). The work of MNC was funded by the EU’s NextGenerationEU instrument through the National Recovery and Resilience Plan of Romania - Pillar III-C9-I8, managed by the Ministry of Research, Innovation and Digitization, within the project entitled “Facets of Rotating Quark-Gluon Plasma” (FORQ), contract no. 760079/23.05.2023 code CF 103/15.11.2022.

- 
- [1] Francesco Becattini, “Spin and polarization: a new direction in relativistic heavy ion physics,” *Rept. Prog. Phys.* **85**, 122301 (2022), [arXiv:2204.01144 \[nucl-th\]](https://arxiv.org/abs/2204.01144).
  - [2] Jian-Hua Gao, Guo-Liang Ma, Shi Pu, and Qun Wang, “Recent developments in chiral and spin polarization effects in heavy-ion collisions,” *Nucl. Sci. Tech.* **31**, 90 (2020), [arXiv:2005.10432 \[hep-ph\]](https://arxiv.org/abs/2005.10432).
  - [3] David Montenegro, Leonardo Tinti, and Giorgio Torrieri, “Ideal relativistic fluid limit for a medium with polarization,” *Phys. Rev. D* **96**, 056012 (2017), [Addendum: *Phys.Rev.D* 96, 079901 (2017)], [arXiv:1701.08263 \[hep-th\]](https://arxiv.org/abs/1701.08263).
  - [4] Wojciech Florkowski, Bengt Friman, Amaresh Jaiswal, and Enrico Speranza, “Relativistic fluid dynamics with

- spin,” *Phys. Rev. C* **97**, 041901 (2018), arXiv:1705.00587 [nucl-th].
- [5] Xu-Guang Huang, “An introduction to relativistic spin hydrodynamics,” (2024), arXiv:2411.11753 [nucl-th].
- [6] L. Adamczyk *et al.* (STAR), “Global  $\Lambda$  hyperon polarization in nuclear collisions: evidence for the most vortical fluid,” *Nature* **548**, 62–65 (2017), arXiv:1701.06657 [nucl-ex].
- [7] S. J. Barnett, “Magnetization by rotation,” *Phys. Rev.* **6**, 239–270 (1915).
- [8] Hao-Lei Chen, Kenji Fukushima, Xu-Guang Huang, and Kazuya Mameda, “Analogy between rotation and density for Dirac fermions in a magnetic field,” *Phys. Rev. D* **93**, 104052 (2016), arXiv:1512.08974 [hep-ph].
- [9] Yin Jiang and Jinfeng Liao, “Pairing Phase Transitions of Matter under Rotation,” *Phys. Rev. Lett.* **117**, 192302 (2016), arXiv:1606.03808 [hep-ph].
- [10] M. N. Chernodub and Shinya Gongyo, “Interacting fermions in rotation: chiral symmetry restoration, moment of inertia and thermodynamics,” *JHEP* **01**, 136 (2017), arXiv:1611.02598 [hep-th].
- [11] M. N. Chernodub and Shinya Gongyo, “Effects of rotation and boundaries on chiral symmetry breaking of relativistic fermions,” *Phys. Rev. D* **95**, 096006 (2017), arXiv:1702.08266 [hep-th].
- [12] Xinyang Wang, Minghua Wei, Zhibin Li, and Mei Huang, “Quark matter under rotation in the NJL model with vector interaction,” *Phys. Rev. D* **99**, 016018 (2019), arXiv:1808.01931 [hep-ph].
- [13] Xun Chen, Lin Zhang, Danning Li, Defu Hou, and Mei Huang, “Gluodynamics and deconfinement phase transition under rotation from holography,” *JHEP* **07**, 132 (2021), arXiv:2010.14478 [hep-ph].
- [14] Anastasia A. Golubtsova and Nikita S. Tsegelnik, “Probing the holographic model of  $N=4$  SYM rotating quark-gluon plasma,” *Phys. Rev. D* **107**, 106017 (2023), arXiv:2211.11722 [hep-th].
- [15] Shi Chen, Kenji Fukushima, and Yusuke Shimada, “Perturbative Confinement in Thermal Yang-Mills Theories Induced by Imaginary Angular Velocity,” *Phys. Rev. Lett.* **129**, 242002 (2022), arXiv:2207.12665 [hep-ph].
- [16] Pracheta Singha, Victor E. Ambrus, and Maxim N. Chernodub, “Inhibition of the splitting of the chiral and deconfinement transition due to rotation in QCD: The phase diagram of the linear sigma model coupled to Polyakov loops,” *Phys. Rev. D* **110**, 094053 (2024), arXiv:2407.07828 [hep-ph].
- [17] Yin Jiang, “Rotating  $SU(2)$  gluon matter and deconfinement at finite temperature,” *Phys. Lett. B* **853**, 138655 (2024), arXiv:2312.06166 [hep-th].
- [18] Fei Sun, Kun Xu, and Mei Huang, “Splitting of chiral and deconfinement phase transitions induced by rotation,” *Phys. Rev. D* **108**, 096007 (2023), arXiv:2307.14402 [hep-ph].
- [19] Hao-Lei Chen, Zhi-Bin Zhu, and Xu-Guang Huang, “Quark-meson model under rotation: A functional renormalization group study,” *Phys. Rev. D* **108**, 054006 (2023), arXiv:2306.08362 [hep-ph].
- [20] Yan-Qing Zhao, Song He, Defu Hou, Li Li, and Zhibin Li, “Phase diagram of holographic thermal dense QCD matter with rotation,” *JHEP* **04**, 115 (2023), arXiv:2212.14662 [hep-ph].
- [21] Gopal Yadav, “Deconfinement temperature of rotating QGP at intermediate coupling from M-theory,” *Phys. Lett. B* **841**, 137925 (2023), arXiv:2203.11959 [hep-th].
- [22] Nelson R. F. Braga, Luiz F. Faulhaber, and Octavio C. Junqueira, “Confinement-deconfinement temperature for a rotating quark-gluon plasma,” *Phys. Rev. D* **105**, 106003 (2022), arXiv:2201.05581 [hep-th].
- [23] S. M. A. Tabatabaee Mehr and F. Taghinavaz, “Chiral phase transition of a dense, magnetized and rotating quark matter,” *Annals Phys.* **454**, 169357 (2023), arXiv:2201.05398 [hep-ph].
- [24] N. Sadooghi, S. M. A. Tabatabaee Mehr, and F. Taghinavaz, “Inverse magnetorotational catalysis and the phase diagram of a rotating hot and magnetized quark matter,” *Phys. Rev. D* **104**, 116022 (2021), arXiv:2108.12760 [hep-ph].
- [25] Yuki Fujimoto, Kenji Fukushima, and Yoshimasa Hidaka, “Deconfining Phase Boundary of Rapidly Rotating Hot and Dense Matter and Analysis of Moment of Inertia,” *Phys. Lett. B* **816**, 136184 (2021), arXiv:2101.09173 [hep-ph].
- [26] Zheng Zhang, Chao Shi, Xiao-Tao He, Xiaofeng Luo, and Hong-Shi Zong, “Chiral phase transition inside a rotating cylinder within the Nambu–Jona-Lasinio model,” *Phys. Rev. D* **102**, 114023 (2020), arXiv:2012.01017 [hep-ph].
- [27] Yidian Chen, Danning Li, and Mei Huang, “Inhomogeneous chiral condensation under rotation in the holographic QCD,” *Phys. Rev. D* **106**, 106002 (2022), arXiv:2208.05668 [hep-ph].
- [28] V. V. Braguta, A. Yu. Kotov, D. D. Kuznedev, and A. A. Roenko, “Study of the Confinement/Deconfinement Phase Transition in Rotating Lattice  $SU(3)$  Gluodynamics,” *JETP Lett.* **112**, 6–12 (2020).
- [29] V. V. Braguta, A. Yu. Kotov, D. D. Kuznedev, and A. A. Roenko, “Influence of relativistic rotation on the confinement-deconfinement transition in gluodynamics,” *Phys. Rev. D* **103**, 094515 (2021), arXiv:2102.05084 [hep-lat].
- [30] M. N. Chernodub, V. A. Goy, and A. V. Molochkov, “Inhomogeneity of a rotating gluon plasma and the Tolman-Ehrenfest law in imaginary time: Lattice results for fast imaginary rotation,” *Phys. Rev. D* **107**, 114502 (2023), arXiv:2209.15534 [hep-lat].
- [31] Victor V. Braguta, Maxim N. Chernodub, Artem A. Roenko, and Dmitrii A. Sychev, “Negative moment of inertia and rotational instability of gluon plasma,” *Phys. Lett. B* **852**, 138604 (2024), arXiv:2303.03147 [hep-lat].
- [32] V. V. Braguta, I. E. Kudrov, A. A. Roenko, D. A. Sychev, and M. N. Chernodub, “Lattice Study of the Equation of State of a Rotating Gluon Plasma,” *JETP Lett.* **117**, 639–644 (2023).
- [33] Victor V. Braguta, Maxim N. Chernodub, Ilya E. Kudrov, Artem A. Roenko, and Dmitrii A. Sychev, “Negative Barnett effect, negative moment of inertia of the gluon plasma, and thermal evaporation of the chromomagnetic condensate,” *Phys. Rev. D* **110**, 014511 (2024), arXiv:2310.16036 [hep-ph].
- [34] Victor V. Braguta, Maxim N. Chernodub, and Artem A. Roenko, “New mixed inhomogeneous phase in vortical gluon plasma: First-principle results from rotating  $SU(3)$  lattice gauge theory,” *Phys. Lett. B* **855**, 138783 (2024), arXiv:2312.13994 [hep-lat].
- [35] V. V. Braguta, M. N. Chernodub, Ya. A. Gershtein, and A. A. Roenko, “On the origin of mixed inhomogeneous phase in vortical gluon plasma,” (2024),

- arXiv:2411.15085 [hep-lat].
- [36] V. V. Braguta, Andrey Kotov, Artem Roenko, and Dmitry Sychev, “Thermal phase transitions in rotating QCD with dynamical quarks,” *PoS LATTICE2022*, 190 (2023), arXiv:2212.03224 [hep-lat].
- [37] Ji-Chong Yang and Xu-Guang Huang, “QCD on Rotating Lattice with Staggered Fermions,” (2023), arXiv:2307.05755 [hep-lat].
- [38] Sergio Morales-Tejera, Victor E. Ambrus, and Maxim N. Chernodub, “Firewall boundaries and mixed phases of rotating quark matter in linear sigma model,” (2025), arXiv:2502.19087 [nucl-th].
- [39] Victor E. Ambrus and M. N. Chernodub, “Vortical effects in Dirac fluids with vector, chiral and helical charges,” *Eur. Phys. J. C* **83**, 111 (2023), [Erratum: *Eur.Phys.J.C* 84, 289 (2024)], arXiv:1912.11034 [hep-th].
- [40] M. N. Chernodub and Victor E. Ambrus, “Phase diagram of helically imbalanced QCD matter,” *Phys. Rev. D* **103**, 094015 (2021), arXiv:2005.03575 [hep-th].
- [41] F. Becattini, Wojciech Florkowski, and Enrico Speranza, “Spin tensor and its role in non-equilibrium thermodynamics,” *Phys. Lett. B* **789**, 419–425 (2019), arXiv:1807.10994 [hep-th].
- [42] Enrico Speranza and Nora Weickgenannt, “Spin tensor and pseudo-gauges: from nuclear collisions to gravitational physics,” *Eur. Phys. J. A* **57**, 155 (2021), arXiv:2007.00138 [nucl-th].
- [43] Kenji Fukushima and Shi Pu, “Spin hydrodynamics and symmetric energy-momentum tensors – A current induced by the spin vorticity –,” *Phys. Lett. B* **817**, 136346 (2021), arXiv:2010.01608 [hep-th].
- [44] Matteo Buzzegoli and Andrea Palermo, “Emergent Canonical Spin Tensor in the Chiral-Symmetric Hot QCD,” *Phys. Rev. Lett.* **133**, 262301 (2024), arXiv:2407.14345 [hep-ph].
- [45] Paul C. W. Davies, Tevian Dray, and Corinne A. Manogue, “The Rotating quantum vacuum,” *Phys. Rev. D* **53**, 4382–4387 (1996), arXiv:gr-qc/9601034.
- [46] M. N. Chernodub and A. S. Nedelin, “Phase diagram of chirally imbalanced QCD matter,” *Phys. Rev. D* **83**, 105008 (2011), arXiv:1102.0188 [hep-ph].
- [47] V. V. Braguta and A. Yu. Kotov, “Catalysis of Dynamical Chiral Symmetry Breaking by Chiral Chemical Potential,” *Phys. Rev. D* **93**, 105025 (2016), arXiv:1601.04957 [hep-th].
- [48] M. Ruggieri and G. X. Peng, “Critical Temperature of Chiral Symmetry Restoration for Quark Matter with a Chiral Chemical Potential,” *J. Phys. G* **43**, 125101 (2016), arXiv:1602.05250 [hep-ph].
- [49] T. G. Khunjua, K. G. Klimenko, and R. N. Zhokhov, “Chiral imbalanced hot and dense quark matter: NJL analysis at the physical point and comparison with lattice QCD,” *Eur. Phys. J. C* **79**, 151 (2019), arXiv:1812.00772 [hep-ph].
- [50] Marco Ruggieri, Maxim N. Chernodub, and Zhen-Yan Lu, “Topological susceptibility, divergent chiral density and phase diagram of chirally imbalanced QCD medium at finite temperature,” *Phys. Rev. D* **102**, 014031 (2020), arXiv:2004.09393 [hep-ph].
- [51] Li-Kang Yang, Xiao-Feng Luo, Jorge Segovia, and Hong-Shi Zong, “A Brief Review of Chiral Chemical Potential and Its Physical Effects,” *Symmetry* **12**, 2095 (2020).
- [52] V. V. Braguta, V. A. Goy, E. M. Ilgenfritz, A. Yu. Kotov, A. V. Molochkov, M. Muller-Preussker, and B. Petersson, “Two-Color QCD with Non-zero Chiral Chemical Potential,” *JHEP* **06**, 094 (2015), arXiv:1503.06670 [hep-lat].
- [53] V. V. Braguta, E. M. Ilgenfritz, A. Yu. Kotov, B. Petersson, and S. A. Skinderev, “Study of QCD Phase Diagram with Non-Zero Chiral Chemical Potential,” *Phys. Rev. D* **93**, 034509 (2016), arXiv:1512.05873 [hep-lat].
- [54] N. Yu. Astrakhantsev, V. V. Braguta, A. Yu. Kotov, D. D. Kuznedev, and A. A. Nikolaev, “Lattice study of QCD at finite chiral density: topology and confinement,” *Eur. Phys. J. A* **57**, 15 (2021), arXiv:1902.09325 [hep-lat].
- [55] Arata Yamamoto and Yuji Hirono, “Lattice QCD in rotating frames,” *Phys. Rev. Lett.* **111**, 081601 (2013), arXiv:1303.6292 [hep-lat].
- [56] Y. Iwasaki, “Renormalization group analysis of lattice theories and improved lattice action: Two-dimensional non-linear O(N) sigma model,” *Nucl. Phys. B* **258**, 141–156 (1985).
- [57] B. Sheikholeslami and R. Wohlert, “Improved Continuum Limit Lattice Action for QCD with Wilson Fermions,” *Nucl. Phys. B* **259**, 572 (1985).
- [58] Y. Maezawa, N. Ukita, S. Aoki, S. Ejiri, T. Hatsuda, N. Ishii, and K. Kanaya (WHOT-QCD), “Heavy-quark free energy, debye mass, and spatial string tension at finite temperature in two flavor lattice QCD with Wilson quark action,” *Phys. Rev. D* **75**, 074501 (2007), arXiv:hep-lat/0702004.
- [59] S. Ejiri, Y. Maezawa, N. Ukita, S. Aoki, T. Hatsuda, N. Ishii, K. Kanaya, and T. Umeda (WHOT-QCD), “Equation of State and Heavy-Quark Free Energy at Finite Temperature and Density in Two Flavor Lattice QCD with Wilson Quark Action,” *Phys. Rev. D* **82**, 014508 (2010), arXiv:0909.2121 [hep-lat].
- [60] A. Ali Khan *et al.* (CP-PACS), “Phase structure and critical temperature of two flavor QCD with renormalization group improved gauge action and clover improved Wilson quark action,” *Phys. Rev. D* **63**, 034502 (2000), arXiv:hep-lat/0008011.
- [61] A. Ali Khan *et al.* (CP-PACS), “Dynamical quark effects on light quark masses,” *Phys. Rev. Lett.* **85**, 4674 (2000), [Erratum: *Phys.Rev.Lett.* 90, 029902 (2003)], arXiv:hep-lat/0004010.
- [62] A. Ali Khan *et al.* (CP-PACS), “Equation of state in finite temperature QCD with two flavors of improved Wilson quarks,” *Phys. Rev. D* **64**, 074510 (2001), arXiv:hep-lat/0103028.
- [63] A. Ali Khan *et al.* (CP-PACS), “Light hadron spectroscopy with two flavors of dynamical quarks on the lattice,” *Phys. Rev. D* **65**, 054505 (2002), [Erratum: *Phys.Rev.D* 67, 059901 (2003)], arXiv:hep-lat/0105015.
- [64] Y. Aoki, G. Endrodi, Z. Fodor, S. D. Katz, and K. K. Szabo, “The Order of the quantum chromodynamics transition predicted by the standard model of particle physics,” *Nature* **443**, 675–678 (2006), arXiv:hep-lat/0611014.
- [65] Claudio Bonati, Massimo D’Elia, Marco Mariti, Michele Mesiti, Francesco Negro, and Francesco Sanfilippo, “Curvature of the chiral pseudocritical line in QCD: Continuum extrapolated results,” *Phys. Rev. D* **92**, 054503 (2015), arXiv:1507.03571 [hep-lat].
- [66] B. B. Brandt, G. Endrodi, and S. Schmalzbauer, “QCD phase diagram for nonzero isospin-asymmetry,” *Phys. Rev. D* **97**, 054514 (2018), arXiv:1712.08190 [hep-lat].
- [67] Bastian B. Brandt and Gergely Endrodi, “QCD phase

- diagram with isospin chemical potential,” [PoS LATTICE2016, 039 \(2016\)](#), [arXiv:1611.06758 \[hep-lat\]](#).
- [68] Szabolcs Borsányi, Zoltán Fodor, Jana N. Guenther, Ruben Kara, Paolo Parotto, Attila Pásztor, Ludovica Pirelli, and Chik Him Wong, “Chiral versus deconfinement properties of the QCD crossover: Differences in the volume and chemical potential dependence from the lattice,” [Phys. Rev. D \*\*111\*\*, 014506 \(2025\)](#).
- [69] Xiangdong Ji, Feng Yuan, and Yong Zhao, “What we know and what we don’t know about the proton spin after 30 years,” [Nature Rev. Phys. \*\*3\*\*, 27–38 \(2021\)](#), [arXiv:2009.01291 \[hep-ph\]](#).